# Modeling of anomalous shift and asymmetric hysteresis behavior of ferroelectric thin films

C. K. Wong and F. G. Shin

Citation: J. Appl. Phys. **96**, 6648 (2004); doi: 10.1063/1.1810634
View online: http://dx.doi.org/10.1063/1.1810634
View Table of Contents: http://jap.aip.org/resource/1/JAPIAU/v96/i11
Published by the American Institute of Physics.

# Modeling of anomalous shift and asymmetric hysteresis behavior of ferroelectric thin films

C. K. Wong[a)]
*Department of Applied Physics, The Hong Kong Polytechnic University, Hong Kong, China*

F. G. Shin
*Department of Applied Physics, Materials Research Center and Center for Smart Materials, The Hong Kong Polytechnic University, Hong Kong, China*

(Received 20 May 2004; accepted 6 September 2004)

An analytical bilayer model has been developed to consider the effect of the existence of a dead layer (e.g., due to polarization degradation) at the film-electrode interface in an otherwise homogeneous ferroelectric thin film. By introducing asymmetric conductivity in the dead layer, the anomalous horizontal (along the field axis) shift behavior of hysteresis loops in ferroelectric thin films is successfully reproduced. Assuming that the ferroelectric *P-E* hysteresis loops of the layers are parallelogramlike, explicit expressions are derived for calculating the internal fields in the film, as well as the "apparent" *D-E* loop as measured from a Sawyer-Tower circuit. The general switching sequence for the ferroelectric phases will be considered. Using the ferroelectric-ferroelectric bilayer model, other anomalous phenomena, including vertical shift and deformed loop shape are also modeled. © *2004 American Institute of Physics*. [DOI: 10.1063/1.1810634]

## I. INTRODUCTION

The hysteresis behaviors of ferroelectric thin films have attracted great research interest for many years. Their bistable polarization as well as small size are promising characters for developing compact nonvolatile memories. Research studies of the anomalous effects and degradation mechanisms in the hysteresis behavior of ferroelectric thin films are essential for device applications. One of the most notable phenomenon is the large voltage offset along the horizontal (electric-field) axis found in the hysteresis loop measurements.[1–11] The result is a deformed hysteresis loop with asymmetric switching.[6] Many researchers attributed the shift effect to the internal field caused by trapped charge carriers.[1–4] Other explanations included domain pinning,[5,6] rectifying effects formed at the ferroelectric-electrode interface,[7–9] and the effect of passive layers.[10–12] It seems that there is no general agreement on a definitive mechanism and that the voltage shift may possibly arise from multiple sources. In addition, many previously suggested mechanisms have not been fully examined by accurate physical models or simulations. Theoretical models have played key roles in providing deeper insight and different approaches have been proposed; Baudry used a lattice model to simulate the shifted hysteresis loop and considered the effect of a nonuniform space charge by means of a doping layer.[13] Lee *et al.* modeled the shifted *P-E* loops with asymmetric electrode materials.[14] Lo and Chen demonstrated the effects of space charge and Schottky barrier heights on asymmetric hysteresis loops. They suggested that the difference of Schottky barrier heights in electrode materials is the origin of a horizontal shift along the field axis.[15] Abe *et al.* proposed the existence of an irreversible polarization layer between the sample and bottom electrode. One state of the polarization will then be more stable than the other and hence cause the shifted *P-E* loop.[11] Recently, Lü and Cao introduced asymmetric surface layers to represent the case of one easy polarization direction. The modeled asymmetry in the hysteresis loop is due to the nonscreened depolarization field.[12] In the absence of a general agreement of the origin(s), we believe that the current theoretical understanding of the shift phenomenon can benefit from further ideas and models.

This work attempts to model this offset phenomenon by introducing a passive dielectric/ferroelectric layer at the film-electrode interface to account for the interfacial inhomogeneity. The passive layer (or dead layer) is a small region in the thin film of effectively nonferroelectric/weak ferroelectric nature. We demonstrate that when the passive layer possesses asymmetric electrical conductivities, which may, e.g., result from the Schottky contact, anomalous horizontal shifts of hysteresis loops are produced. Actually, approaches involving asymmetric conductivity have been applied to study the vertical shift observed in graded ferroelectrics.[16–18] This mechanism leading to asymmetric leakage current has long been observed and discussed in literature.[7–9,19,20] The accumulated interfacial charge will allow the buildup of an internal bias field to displace the hysteresis loop from the origin.

In this article, we propose to use the ferroelectric-dielectric and ferroelectric-ferroelectric bilayer structures to model a thin film with passive layers. The ferroelectric loops of the different layers are modeled by parallelogramlike hysteresis loops. This usage allows us to obtain closed-form solutions for the differential equations which are otherwise difficult to solve. A generalized explicit expression for the electric field is then derived and is already sufficient to tackle all different regimes of time of the ferroelectric loops for both phases. Our model simulates the dynamic measurement of hysteresis loop and the results clearly reveal the accumu-

[a)]Electronic mail: wongck.a@polyu.edu.hk

 

lation of charge as well as the time development of electric fields. We demonstrate that the horizontal offset is strongly dependent on the asymmetry of electrical conductivities, thickness of passive layer, and the applied ac field. Other effects including the permittivity and ferroelectric polarization are also discussed. Lastly, the ferroelectric–ferroelectric bilayer model is used to illustrate other degradation phenomena including vertically shifted and asymmetrically deformed hysteresis loops.

## II. THEORY

Our model assumes that a passive layer is formed at the ferroelectric film sample-electrode interface. This passive layer (or dead layer) is a region adjacent to the electrode with a large drop in remanent polarization below the bulk value (i.e., a weak ferroelectric/dielectric layer).[21–23] Although the origin of the dead layer formation may still be under debate,[21] it has been pointed out that the dead layer is an intrinsic effect in ferroelectric thin films.[22] Although the dead layer effect may take place at both sample–electrode interfaces, we include the overall effect in a single passive layer for convenience. Therefore, a ferroelectric thin film with a dead layer can be modeled by a double-layer structure. The constitutive equations are

$$D_f = \varepsilon_f E_f + P_f, \qquad D_d = \varepsilon_d E_d + P_d, \tag{1}$$

where $D$ is electric displacement, $P$ is polarization, $\varepsilon$ is permittivity, and $E$ is electric field. Subscripts $f$ and $d$ denote the bulk layer (normal region of the film) and dead layer, respectively.

When an external electric field $E_a$ is applied in the thickness direction across the film,

$$E_a = (1-\nu)E_f + \nu E_d, \tag{2}$$

where $\nu$ represents the thickness ratio of the dead layer in the thin-film. Suppose the thin film material supports a finite conductivity so that charge may flow. Thus, the boundary conditions for the continuity of current density require

$$J_f = J_d = \sigma_f^{\pm} E_f + \frac{\partial D_f}{\partial t} = \sigma_d^{\pm} E_d + \frac{\partial D_d}{\partial t}, \tag{3}$$

where $\sigma$ is electrical conductivity and $J$ denotes current density, inclusive of conduction and displacement currents. Following the notation adopted by Bouregba *et al.*[17] and Zheng *et al.*,[24] $\sigma_f$ and $\sigma_d$ may take different values for positive (represented by superscript "+") and negative (represented by superscript "−") internal electric fields. Using Eqs. (1)–(3), we obtain, after some manipulation,

$$\frac{\partial E_f}{\partial t} + \frac{E_f}{\tau^{\pm}} = \zeta\left(\frac{E_a}{\tau_d^{\pm}} + \frac{\partial E_a}{\partial t}\right), \tag{4}$$

where

$$\zeta^{-1} = 1 - \nu\left(1 - \frac{\varepsilon_f + \partial P_f/\partial E_f}{\varepsilon_d + \partial P_d/\partial E_d}\right), \tag{5}$$

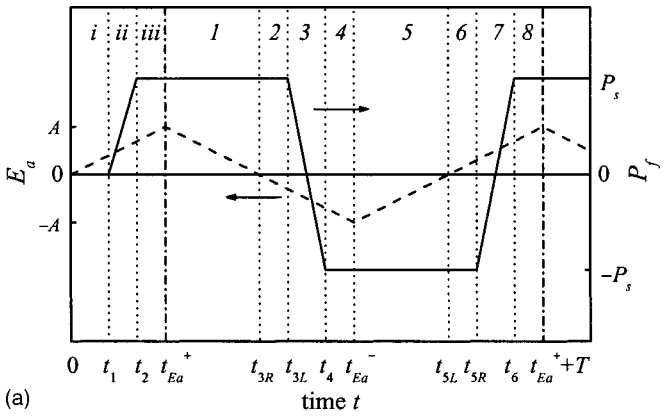


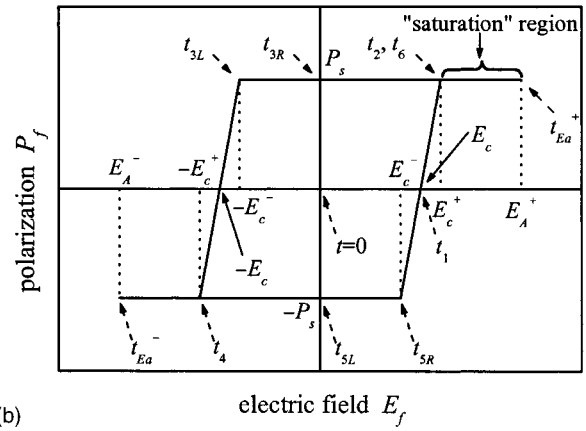


FIG. 1. The variation of the applied field $E_a$ (dashed line) and polarization $P_f$ (solid line) with time. Regimes i–iii belong to the initial region and regimes 1–8 are for the looping region. (b) A multilinear, parallelogramlike $P_f$-$E_f$ hysteresis loop.

$$\tau^{\pm} = \frac{\nu(\varepsilon_f + \partial P_f/\partial E_f) + (1-\nu)(\varepsilon_d + \partial P_d/\partial E_d)}{\nu\sigma_f^{\pm} + (1-\nu)\sigma_d^{\pm}}, \tag{6}$$

and $\tau_d^{\pm} = \varepsilon_d/\sigma_d^{\pm}$. For a given external ac field $E_a$, we may obtain $E_f$ as a function of time $t$ when the $P$-$E$ relation for the sample is known. Then the electric displacement of the sample (as measured by a Sawyer-Tower circuit) at a certain time $t_0$ is given by the integration of current density across the (ideal) reference capacitor of large capacity

$$D(t_0) = \int_0^{t_0} J_r dt, \tag{7}$$

where subscript $r$ represents the reference capacitor and $J_r = J_f = J_d$.

### A. Ferroelectric–dielectric layered model

We first consider that the dead layer is nonferroelectric, i.e., $P_d = 0$. Therefore, $\partial P_d/\partial E_d = 0$ in Eqs. (5) and (6). In this work, the applied electric field used is a triangular wave [dashed line in Fig. 1(a)] and the hysteresis loop is taken as a parallelogram [Fig. 1(b)]. Initially, $E_f = 0$ and $P_f = 0$. When $E_f$ increases, we take that $P_f$ remains zero until $t = t_1$ and the time regime for $0 \leqslant t \leqslant t_1$ is denoted as i [Fig. 1(a)]. Thereafter the polarization response is governed by the parallelogram hysteresis loop. Thus, in regime ii ($t_1 \leqslant t \leqslant t_2$), $P_f$ increases linearly [Fig. 1(b)]. For regime iii, $P_f$ reaches its

TABLE I. Representation of symbols in Eqs. (8)–(10) with different regimes defined in Fig. 1 for ferroelectric-dielectric layered structure.

| Regime (Fig. 1) | $t_{\text{init}}$ | $t_{\text{final}}$ [Eq. (9)] | $E_{\text{init}}$ | $E_{\text{final}}$ | $\partial P_f/\partial E_f$ (in $\zeta$ and $\tau^{\pm}$) | $\alpha$ | $\delta$ | $t_{Ea}^{\mp}$ | $\sigma_f^{\pm}$ | $\sigma_d^{\pm}$ |
|---|---|---|---|---|---|---|---|---|---|---|
| i | 0 | $t_1$ | 0 | $E_c$ | 0 | 0 | +1 | 0 | $\sigma_f^+$ | $\sigma_d^+$ |
| ii | $t_1$ | $t_2$ | $E_c$ | $E_c^+$ | $m_f$ | 0 | +1 | 0 | $\sigma_f^+$ | $\sigma_d^+$ |
| iii | $t_2$ | $t_{Ea}^+$ | $E_c^+$ | $E_A^+$ | 0 | 0 | +1 | 0 | $\sigma_f^+$ | $\sigma_d^+$ |
| *1* | $t_{Ea}^+$ | $t_{3R}$ | $E_A^+$ | 0 | 0 | $A$ | −1 | $t_{Ea}^+$ | $\sigma_f^+$ | $\sigma_d^{\pm}$ [a] |
| *2* | $t_{3R}$ | $t_{3L}$ | 0 | $-E_c^-$ | 0 | $A$ | −1 | $t_{Ea}^+$ | $\sigma_f^-$ | $\sigma_d^{\pm}$ [a] |
| *3* | $t_{3L}$ | $t_4$ | $-E_c^-$ | $-E_c^+$ | $m_f$ | $A$ | −1 | $t_{Ea}^+$ | $\sigma_f^-$ | $\sigma_d^{\pm}$ [a] |
| *4* | $t4$ | $t_{Ea}^-$ | $-E_c^+$ | $E_A^-$ | 0 | $A$ | −1 | $t_{Ea}^+$ | $\sigma_f^-$ | $\sigma_d^{\pm}$ [a] |
| *5* | $t_{Ea}^-$ | $t_{5L}$ | $E_A^-$ | 0 | 0 | $A$ | +1 | $t_{Ea}^-$ | $\sigma_f^-$ | $\sigma_d^{\pm}$ [a] |
| *6* | $t_{5L}$ | $t_{5R}$ | 0 | $E_c^-$ | 0 | $A$ | +1 | $t_{Ea}^-$ | $\sigma_f^+$ | $\sigma_d^{\pm}$ [a] |
| *7* | $t_{5R}$ | $t_6$ | $E_c^-$ | $E_c^+$ | $m_f$ | $A$ | +1 | $t_{Ea}^-$ | $\sigma_f^+$ | $\sigma_d^{\pm}$ [a] |
| *8* | $t_6$ | $t_{Ea}^+$ | $E_c^+$ | $E_A^+$ | 0 | $A$ | +1 | $t_{Ea}^-$ | $\sigma_f^+$ | $\sigma_d^{\pm}$ [a] |

[a]Determined by the sign of $E_d$ which can be calculated from Eqs. (2) and (8).

saturation value and remains a constant as $E_f$ increases. The behavior of the polarization in the subsequent full period may be conveniently divided into time regimes *1–8* which correspond to tracing on the hysteresis loop. This behavior repeats itself for further ac cycles. It is seen that $\partial P_f/\partial E_f$ becomes a constant ($\equiv m_f$) for $t_{3L} \leqslant t \leqslant t_4$ or $t_{5R} \leqslant t \leqslant t_6$, and is zero elsewhere. In this model, we have assumed that the field amplitude of $E_f$ is sufficiently large so that the parallelogram loop is traced. Therefore, the time development of $P_f$ is trapezoidlike [solid line in Fig. 1(a)]. Note that each of $\sigma_f$ and $\sigma_d$ may take different values ($\sigma^{\pm}$) for positive and negative driving fields. When $\sigma_d^{\pm}$ is a constant (ohmic conductivity), the solution from solving Eq. (4) with initial condition $E_f(t_{\text{init}}) = E_{\text{init}}$ is

$$E_f(t) = E_{\text{init}}\exp(-(t-t_{\text{init}})/\tau^{\pm}) + \delta\zeta(\tau^{\pm}/\tau_d^{\pm}) \times\{m_a[t + t_{\text{init}}\exp(-(t-t_{\text{init}}(/\tau^{\pm})] - [\alpha + m_a(t_{Ea}^{\mu} + \tau^{\pm} - \tau_d^{\pm})](1-\exp(-(t-t_{init})/\tau^{\pm})]\}, \quad (8)$$

where $m_a = 4A/T$, and $A$ and $T$ represent the amplitude and period of the applied electric field. Equation (8) is a general expression applicable to all time regimes defined in Fig. 1. Symbols $t_{\text{init}}$, $E_{\text{init}}$, $\zeta$, $\alpha$, $\delta$, $t_{Ea}^{\mp}$, $\sigma_f^{\pm}$, and $\sigma_d^{\pm}$ take on different values for different regimes (see Fig. 1), as shown in Table I. In Table I, $E_c^+ = E_c + P_s/m_f$ and $E_c^- = E_c - P_s/m_f$. $E_A^+$ and $E_A^-$ are the electric field across the ferroelectric (bulk) layer in the bilayered film when $E_a = A$ and $-A$, respectively ($t = t_{Ea}^+$ and $t_{Ea}^-$, respectively). Since the value of $\sigma_d$ ($\sigma_d^+$ or $\sigma_d^-$) is dictated by the sign of $E_d$ rather than $E_f$, the latter has to be calculated from the combined use of Eqs. (8) and (2) when tracing the hysteresis loop. Apart from $t_{Ea}^+$ and $t_{Ea}^-$, all $t$'s defined in Fig. 1 depend on the constituent properties of the materials. They may be calculated from the end value of $E_f(\equiv E_{\text{final}})$ for each regime,

$$t_{\text{final}} = \frac{\alpha}{m_a} + t_{Ea}^{\mp} + \tau^{\pm} - \left(1 - \frac{\delta E_{\text{final}}}{\zeta m_a \tau^{\pm}}\right)\tau_d^{\pm} + \tau^{\pm} W_0[\gamma(E_{\text{init}})e^{\gamma(E_{\text{final}})}], \quad (9)$$

where $W_0(z)$ is the principal branch of the Lambert $W$ function [defined as the solutions of $W\exp(W) = z$],[25] and

$$\gamma(E_b) = \frac{\tau_d^{\pm}}{\tau^{\pm}}\left(1 - \frac{\delta E_b}{\zeta m_a \tau^{\pm}} + \frac{t_{\text{init}} - t_{Ea}^{\mp} - \tau^{\pm} - \alpha/m_a}{\tau_d^{\pm}}\right). \quad (10)$$

The values of the symbols in Eq. (9) for calculating different $t_{final}$'s are also shown in Table I. Thus, $E_f$ for the first quarter period can be obtained from Eqs. (8)–(10) with parameters suitable for regimes i–iii, and for the subsequent full period by Eqs. (8)–(10) with parameters suitable for regimes *1–8*. More periods may be calculated repeatedly by applying the equations for regimes *1–8* with $t_{Ea}^+$ and $E_A^+$ updated recursively.

To examine the dynamic behavior of the simulated $D$, the integral of $E_f$ must be calculated in each regime [Eqs. (3) and (7)]. However, this tedious work can be bypassed when $\sigma_f = 0$ which corresponds to a perfectly insulating bulk layer. Equation (6) then reduces to $\tau^{\pm} = \tau_d^{\pm} + [\nu/(1-\nu)][(\varepsilon_f + \partial P_f/\partial E_f)/\sigma_d^{\pm}]$. From Eqs. (1), (3), and (7), the "measured" electric displacement of the sample at a certain time $t_0$ is calculated by

$$D(t_0) = [\varepsilon_f + \chi(t)]E_f(t)|_0^{t_0}, \quad (11)$$

where $\chi(t) \equiv \partial P_f/\partial E_f$ with values of 0 or $m_f$ for the respective regimes (Table I).

### B. Ferroelectric–ferroelectric layered model

For the case of a dead layer having ferroelectric behavior, a ferroelectric–ferroelectric layered model should be considered. Here, two different parallelogramlike hysteresis loops are employed to model the ferroelectricity of the layers with constant $\partial P_f/\partial E_f$ and $\partial P_d/\partial E_d$ throughout each regime. In a ferroelectric-dielectric layered model, there are eight regimes for each loop and the parameters adopted for Eq. (8) other than $\sigma_d$ (listed in Table I) is fixed for each regime (since there is a single path in the hysteresis looping). However, a ferroelectric–ferroelectric layered model will have multiple pathways for each period. This is because the sequence of polarization switching needs to be considered in a model having more than one ferroelectric phase. Figure 2 shows all possible pathways in the switching of a bilayer system with ferroelectric phases. The initial and looping responses can be divided into five and ten regimes, respectively, having one, two, or four possible polarization "states"

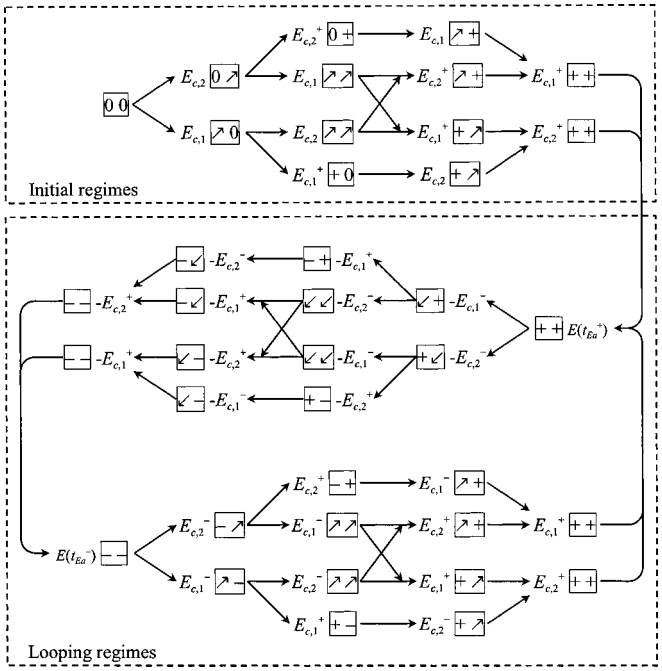


FIG. 2. Flow diagram illustrating all possible polarization states *xy* and switching pathways (→) for the simulation of a ferroelectric–ferroelectric bilayered structure with parallelogramlike *P-E* hysteresis loop for each layer.

*xy* in each time regime. The letters *x* and *y* within the square symbol denote the individual "polarization state" in the layers, say, layer 1 and layer 2, respectively, which may take on one of the five values: "0," "↗," "+," "↙," or "−." We assume that at $t=0$, when the external ac field is applied, both layers have zero polarization, thus the initial state of the bilayer is 00. Subsequently, the field within each layer changes, driving the polarization around its *P-E* loop if the field amplitude is of sufficient magnitude. In this case, the polarization goes successively onto the ascending branch ↗, the top branch +, the descending branch ↙, the bottom branch −, and so forth. For a bilayer, there are many possible *xy* states. For example, in the initial first, second, and third regimes there one, two, and four possible states, respectively. The change from one bilayer state to another, indicated by an arrow, is triggered by the condition that the electric field in one of the layers reaches the critical value for a change. This critical electric field value is also given in Fig. 2 and written in front of a state.

To obtain the internal electric field $E_f$ and then $E_d$, Eqs. (8)–(10) are still applicable. With the help of Fig. 2, it is possible but impracticable to formulate a table (similar to Table I) which lists the meaning carried by $t_{\text{init}}$, $t_{\text{final}}$, $E_{\text{init}}$, $E_{\text{final}}$, $\zeta$, $\alpha$, $\delta$, $t_{Ea}^{\mp}$, $\sigma_f^{\pm}$, and $\sigma_d^{\pm}$ for each time regime. The parameter set is much larger since each regime constitutes one to four states, and the looping regimes constitute 36 paths in a ferroelectric-ferroelectric structure (versus a single path in a ferroelectric-dielectric structure). Also, $\sigma_f$ switches between $\sigma_f^+$ and $\sigma_f^-$ when $E_f$ changes sign, and similarly for $\sigma_d$ when $E_d$ changes. Those ought to be determined by calculating the instantaneous $E_f$ and $E_d$ when applying Eqs. (8) and (2) to trace the two parallelogram loops.

To examine the dynamic behavior of the simulated *D*, Eqs. (3) and (7) are used and $E_f$ and $E_d$ must be calculated for each regime. Equation (11) is used instead when $\sigma_f^{\pm}=0$.

## III. RESULTS AND DISCUSSION

In this section, theoretical predictions based on the foregoing bilayer models for thin films with a dead layer are investigated. In this work, we adopted $E_c^{(f)}=5\ \text{V}/\mu\text{m}$, and also $E_c^{(d)}=5\ \text{V}/\mu\text{m}$ when the passive layer possesses a ferroelectric behavior. Superscripts $(f)$ and $(d)$ are used to differentiate the bulk layer and dead layer of the thin film. In addition, $m_f(\text{for bulk layer})=m_d(\text{for passive layer})=50\times10^{-8}\ \text{Fm}^{-1}$. Table II shows all the other adopted values for the properties of the bulk and passive layers in the ferroelectric thin film, as well as the applied field parameters, for our predictions in each figure. In Table II, $\varepsilon_0$ is the permittivity of vacuum.

### A. Asymmetric conductivity induced horizontally shifted hysteresis loop and the effect of film thickness

Many researchers believed that the horizontally shifted hysteresis loop is the result of an internal biased field developed across the ferroelectric film. Indeed, our modeling results will show a strong dc biased field developed across the passive layer in thin film, as well as an asymmetric development of charges with time. The magnitude of the biased field, which leads to the shifted hysteresis loop, strongly depends on the asymmetry of conductivity in the passive layer ($\sigma_d^+$ and $\sigma_d^-$). A lower film permittivity (which may arise from the finite-size effect of ferroelectric films) will also enhance the biased field and the asymmetric effect of hysteresis loop.

TABLE II. The magnitude and period of applied field, and the properties of the sample used in the calculations.

| Fig. | $A$ ($\text{V}\,\mu\text{m}^{-1}$) | $T$ (s) | $\nu$ | $P_s^{(f)}$ ($\mu\text{C cm}^{-2}$) | $\varepsilon_f/\varepsilon_0$ | $\sigma_f^+$ ($10^{-11}\ \Omega^{-1}\,\text{cm}^{-1}$) | $\sigma_f^-$ ($10^{-11}\ \Omega^{-1}\,\text{cm}^{-1}$) | $P_s^{(d)}$ ($\mu\text{C cm}^{-2}$) | $\varepsilon_d/\varepsilon_0$ | $\sigma_d^+$ ($10^{-10}\ \Omega^{-1}\,\text{cm}^{-1}$) | $\sigma_d^-$ ($10^{-10}\ \Omega^{-1}\,\text{cm}^{-1}$) |
|---|---|---|---|---|---|---|---|---|---|---|---|
| 3(a) | 20 | 0.01 | 0.05 | 20 | 300 | 0 | 0 | nil | 300 | varied | varied |
| 3(b) | 25 | 0.01 | varied | 20 | 300 | 0 | 0 | nil | 300 | 0.1 | 1 |
| 4 | varied | 0.01 | 0.05 | 20 | 300 | 0 | 0 | nil | 300 | 0.1 | 1 |
| 5 | 20 | 0.1 | 0.05 | 20 | 300 | 0 | 0 | nil | 300 | 0.1 | 1 |
| 6 | 20 | 0.1 | 0.05 | 20 | 300 | 0 | 0 | nil | 300 | 0.1 | 1 |
| 7(a) | 25 | 0.01 | 0.05 | varied | 300 | 0 | 0 | nil | 300 | 0.1 | 1 |
| 7(b) | 25 | 0.02 | 0.1 | 20 | 300 | $10^{-4}$ | $10^{-4}$ | varied | 300 | $10^{-4}$ | 1 |
| 8 | 45 | 0.02 | 0.01 | 20 | varied | $10^{-2}$ | $10^{-2}$ | $10^{-3}$ | varied | $10^{-2}$ | 1 |
| 9 | 20 | 0.02 | 0.05 | 20 | 300 | varied | varied | $10^{-3}$ | 300 | 0.1 | 1 |

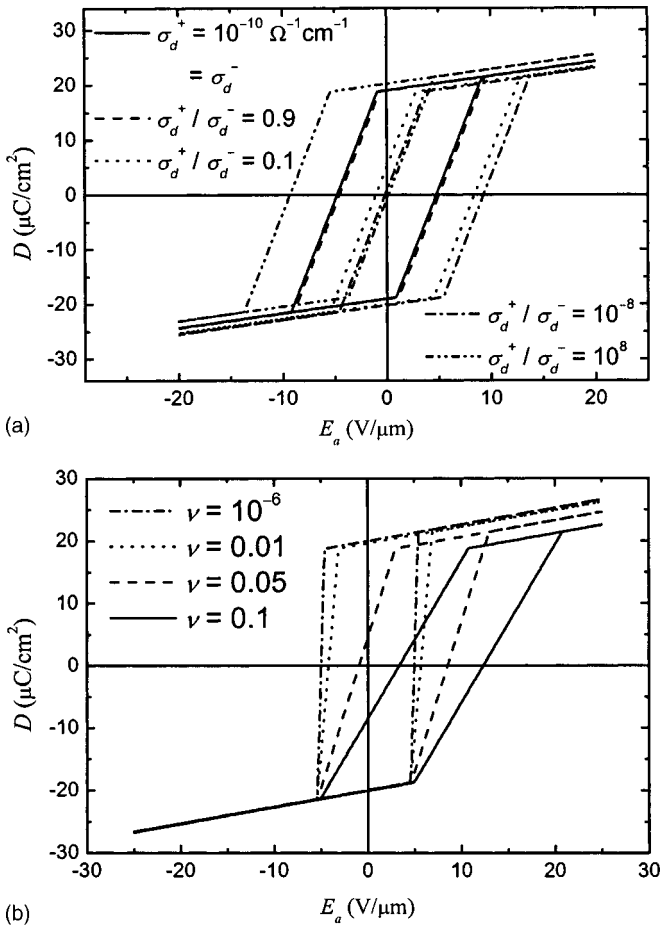


FIG. 3. Variations of the simulated *D-E* hysteresis loop with (a) the asymmetry of conductivity in passive layer and (b) the thickness ratio of passive layer.

Figure 3(a) shows the simulated results of the *D-E* hysteresis loop for a ferroelectric thin film with a nonferroelectic passive layer. Different pairs of asymmetric $\sigma_d$ have been adopted to demonstrate the horizontal shift phenomenon. The bulk layer of the ferroelectric film is taken as an insulator (i.e., $\sigma_f=0$). In the figure, all the modeled results are picked at 3 s after the application of the external ac field, at which time the horizontal shift of these loops should be extremely close to their steady-state value. When the passive layer has symmetric conductivity ($\sigma_d^+=\sigma_d^-=10^{-10}\ \Omega^{-1}\,\text{cm}^{-1}$), the hysteresis loop centers at the origin and no horizontal and vertical shifts are observed. Suppose $\sigma_d^-$ remains at $10^{-10}\ \Omega^{-1}\,\text{cm}^{-1}$ and $\sigma_d^+/\sigma_d^-\neq 1$ so that asymmetry in conductivity is introduced into the passive layer, then significant horizontal shift is observed. The magnitude of the horizontal shift increases as asymmetry in $\sigma_d$ increases. Note that, when $\sigma_d^+$ is smaller than $\sigma_d^-$ by an order, an almost maximum horizontal shift is achieved. Any further reduction in $\sigma_d^+$ will have little effect in the horizontal shift. When the values for $\sigma_d^+$ and $\sigma_d^-$ are interchanged, the hysteresis loop shifts to the opposite direction with an unchanged shift magnitude. In the above, our adopted conductivity values might be somewhat higher than typical values, but we found that the shift behavior was almost identical for the same asymmetry ratio with smaller $\sigma_d^+$ and $\sigma_d^-$, only it generally took more cycles to reach the steady state. Figure 3(b) shows the effect of thickness ratio of the passive layer on the hysteresis loop. For a thick ferroelectric film, the effect of surface and film–electrode interaction is limited. This corresponds to a thin passive layer, i.e., $\nu$ is small, and we assume $\nu=10^{-6}$ in our simulation. The hysteresis loop almost centers at the origin and no notable horizontal and vertical shifts are observed. Suppose $\nu=1\%$ and the nonferroelectric passive layer possesses asymmetric conductivity, then the simulated hysteresis loops start to twist to one side. The skewed loop thus has unequal magnitudes of coercive fields, giving an apparent horizontal shift. As $\nu$ increases, the horizontal "shift" increases.

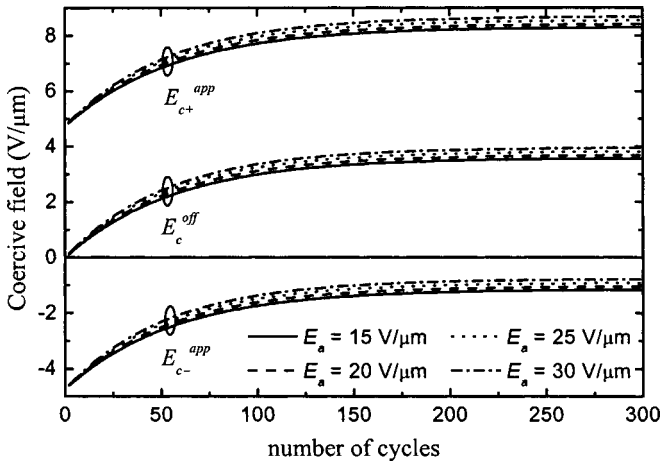


FIG. 4. Time development of the simulated coercive fields ($E_{c^+}^{app}$ and $E_{c^-}^{app}$) and the horizontal offset of hysteresis loop ($E_c^{off}$). Four different amplitudes of applied fields have been shown.

### B. Time development of coercive fields and the effect of applied field amplitude

Indeed, the large horizontal shift phenomenon may not occur immediately in a few cycles of measurement. The time dependence of the simulated coercive fields ($E_{c^+}^{\text{app}}$ and $E_{c^-}^{\text{app}}$) and horizontal shift magnitude $E_c^{\text{off}}$ [$\equiv(E_{c^+}^{\text{app}}+E_{c^-}^{\text{app}})/2$] are shown in Fig. 4. Initially, $E_{c^+}^{\text{app}}$ and $E_{c^-}^{\text{app}}$ are symmetric to each other with magnitudes slightly less than 5 V/$\mu$m (since the passive layer is nonferroelectric). As more ac cycles are simulated, the coercive fields $E_c^{\text{app}}$ increase gradually until saturation. Thus, the horizontal shift $E_c^{\text{off}}$ of the loop takes time to reach saturation. Different applied field amplitudes are also shown in Fig. 4. In general, the horizontal shift increases as the amplitude of $E_a$ increases. This effect only translates the whole loop further to one side, since the resulting loop width $E_{c^+}^{\text{app}}-E_{c^-}^{\text{app}}$ remains almost the same. The phenomena of shift and skewed hysteresis loop demonstrated in Fig. 3 are the results of the existence of a dynamic dc electric field in the passive layer. Figure 5 shows the time development of the electric fields in the bulk ferroelectric layer ($E_f$) and the nonferroelectric passive layer ($E_d$). The phenomenon of a progressive buildup of interfacial charge density ($=D_d-D_f$) is shown in Fig. 6. The frequency of the applied field is set at 10 Hz to allow saturation to be reached in fewer field cycles (30 cycles), rather than about 300 cycles for the case

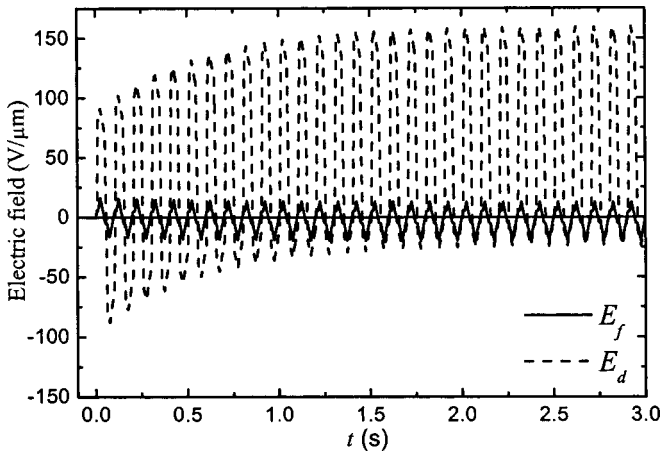


FIG. 5. Theoretical results of the electric fields in the bulk ($E_f$) and passive ($E_d$) layers vs time for $\nu=0.05$. The frequency of the applied field is 10 Hz.

of 100 Hz, even though they all correspond to 3 s. In Fig. 5, the electric-field profile of the bulk ferroelectric layer is almost unchanged with time. However, a dc bias continuously builds up in the passive layer until saturation. This is the effect of asymmetric conductivity, which leads to accumulation of interfacial charge (see Fig. 6). As shown in Fig. 6, the profile of interfacial charge shifts vertically with time with a net offset at saturation. Hence the asymmetric internal field shown in Fig. 5 is thought to display the hysteresis loop from the origin. In the situation that the passive layer has symmetric conductivity, a development of interfacial charge is still observed, but the net offset diminishes to zero for a sufficiently long time, determined by conductivity and frequency of the applied field.

Our results show that the hysteresis loop is right shifted when $\sigma_d^+ < \sigma_d^-$ and left shifted when $\sigma_d^+ > \sigma_d^-$ [see Fig. 3(a)]. In the former case, the rate of interfacial charge development will be slower when the field cycle is in the positive polarity. This promotes a positive dc bias buildup (see Fig. 5) and the hysteresis loop is displaced to the right. In thin-film fabrication, asymmetric conductivity may be due to the different bottom and top electrodes with quite different interface effects. Moreover, even for a ferroelectric film with symmetric electrodes, Zheng *et al.* suggested that the bottom electrode usually received high-temperature cycles during film deposition and postannealing, while the top electrode received less or no heat cycles.[24] Hence different barrier heights may be formed at the bottom and top interfaces, which leads to the asymmetric conductivity characteristic. The value of $\sigma_d^+/\sigma_d^-$, which dictates the magnitude and shift direction, is then believed to behave quite differently for different processing conditions, even for the same composition of ferroelectric.

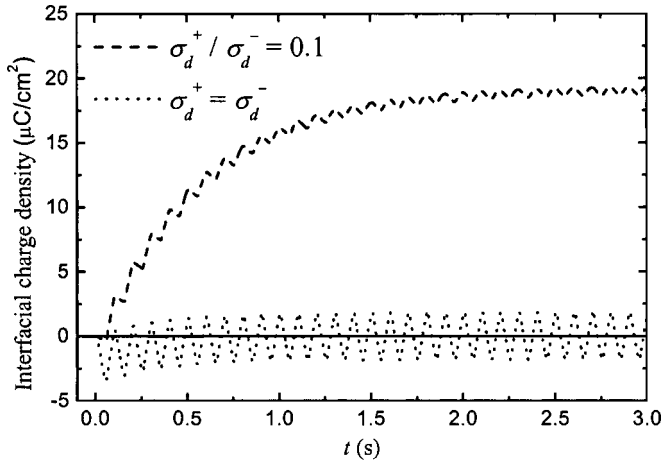


FIG. 6. Effect of the asymmetric conductivity of the passive layer on the time-dependent interfacial charge densities ($=D_d-D_f$) for $\nu=0.05$. The frequency of the applied field is 10 Hz.

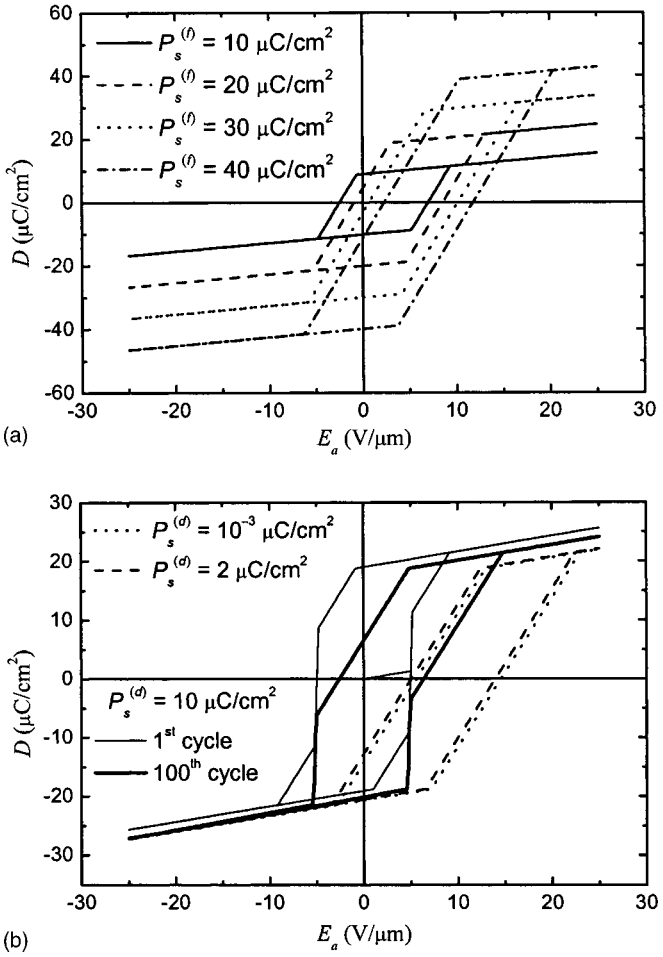


FIG. 7. The variation of the simulated *D-E* hysteresis loop corresponding to different values of $P_s$ in (a) the bulk layer and (b) the passive layer. The first and the last loops when $P_s^{(f)}=20\ \mu C/cm^2$ and $P_s^{(d)}=10\ \mu C/cm^2$ have been shown for comparison.

### C. Effects of ferroelectric polarization and permittivity on the horizontally shifted hysteresis loop

In Fig. 7, the effects of $P_s^{(f)}$ and $P_s^{(d)}$ on the hysteresis loop are separately investigated. Figure 7(a) demonstrates that a large polarization loop in the bulk layer enhances the effect of the horizontal shift phenomenon. However, a larger $P_s^{(d)}$ reduce the shift effect [see Fig. 7(b)]. When the passive layer only has weak ferroelectricity (e.g., $P_s^{(d)}=2\ \mu C/cm^2$, one-tenth of $P_s^{(f)}$), the magnitude of the horizontal shift is still significant. It seems that as $P_s^{(d)}$ increases, the magnitude of the horizontal shift decreases. It is interesting to note that for some larger $P_s^{(d)}$, e.g., $P_s^{(d)}=10\ \mu C/cm^2$ (one-half of $P_s^{(f)}$),

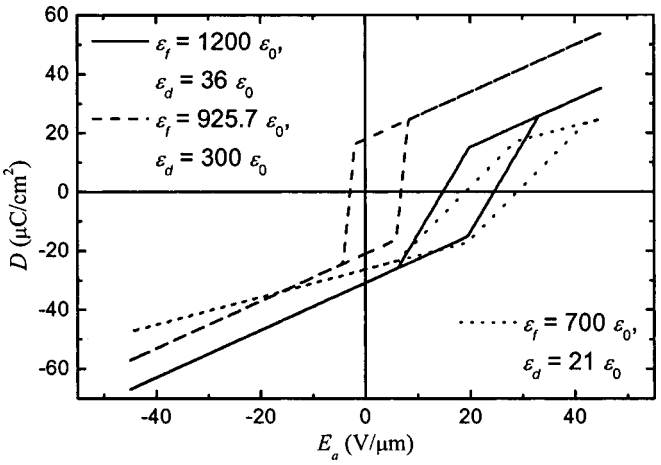


FIG. 8. Effect of the permittivities on the horizontal offset of hysteresis loops. The effective permittivity is identical for the case of solid and dashed lines. The dotted line have adopted the same permittivity ratio ($\varepsilon_f/\varepsilon_d$) as for the solid line, but with lower effective permittivity.

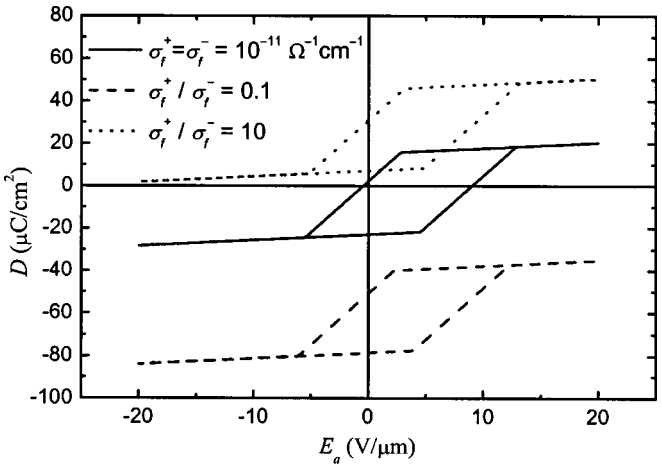


FIG. 9. Variations of the simulated *D-E* hysteresis loop with the asymmetry of conductivity in the bulk layer.

the curve shows a symmetric shape at the first cycle. After 100 cycles of measurement, the loop shape is highly distorted. In this case, the horizontal shift effect may not be so pronounced, but the deformation leading to an asymmetric hysteresis loop is significant.

Comparison with some previous experimental results shows that our simulation results give a generally good agreement in the shift magnitude and loop shape (see Refs. 1–6). On the other hand, some published experimental results demonstrated large magnitudes in horizontal offset,[3,26] and in some extreme cases, the whole hysteresis loop (apart from the tails) might lie on the same side of the field axis. Figure 8 shows that our model can also reproduce similarly large horizontal offsets. In the literature, it is known that the permittivity of ferroelectric thin film decreases with film thickness. The permittivity of thin film will generally be smaller than that for a bulk sample of the same material.[21,27] Therefore, we adopted relatively smaller values for $\varepsilon$ (=300 $\varepsilon_0$) in our previous calculations (Figs. 3–7). In addition, we assumed for convenience $\varepsilon_f = \varepsilon_d$ and had already been able to demonstrate some large offsets. Actually, some researchers proposed that the dead layer should have a significantly smaller permittivity than the bulk layer. Hence the thin-film structure possesses an effectively smaller permittivity value than the bulk sample. As the film thickness reduces, the contribution of small permittivity from the passive layer becomes more significant, resulting in a reduced permittivity for the film. Chen *et al.* proposed 1370 and 42.6 for the dielectric constants of the bulk barium strontium titanate and the dead layers, respectively.[27] Their film thickness ranged from 100 to 300 nm and the dead layer thickness was estimated to be 2.8 nm. Following their findings, we assume $\nu = 0.01$ and $\varepsilon_d/\varepsilon_f = 0.03$. It is then possible to obtain a very large horizontal offset, as shown by the solid line in Fig. 8. This curve corresponds to an effective permittivity $= [\nu/\varepsilon_d + (1-\nu)/\varepsilon_f]^{-1} = 907\ \varepsilon_0$ [from Eqs. (1)–(3)]. In Fig. 8, the dashed line assumes the same effective $\varepsilon$ (=907 $\varepsilon_0$) as the solid line but with $\varepsilon_d = 300\ \varepsilon_0$. This significantly increases the ratio $\varepsilon_d/\varepsilon_f$ and the resultant loop has a small horizontal offset. On the other hand, if we adopt $\varepsilon_f = 700\ \varepsilon_0$ and $\varepsilon_d = 21\ \varepsilon_0$ which also maintains $\varepsilon_d/\varepsilon_f = 0.03$ as in the first case (but the effective dielectric constant becomes 529), the horizontal offset further increases. Overall, it seems that both low $\varepsilon_d/\varepsilon_f$ and low permittivty of film can enhance the effect of horizontal offset.

### D. Asymmetric conductivity induced phenomenon of vertically shifted hysteresis loop

In a previous paper, we have demonstrated that large polarization offsets can originate from asymmetric conductivity in a ferroelectric film.[28] The present model is able to consider the coupled horizontal and vertical offsets. In addition to the asymmetric conductivity in the passive layer, we can further assume that the bulk layer also possesses asymmetric conductivity. Figure 9 shows that a horizontally shifted hysteresis loop also translates upward or downward along the polarization axis depending on whether $\sigma_f^+/\sigma_f^-$ is larger or smaller than one. It is noted that the magnitude of vertical shift for a chosen $\sigma_f^+/\sigma_f^-$ is not identical for a reciprocal $\sigma_f^+/\sigma_f^-$. Indeed, many large polarization offsets observed in graded ferroelectrics possessed unequal shift magnitudes for downgraded and upgraded films.[29] Concerning the origin of asymmetric $\sigma_f$, Bouregba *et al.* suggested that the compositional gradient in a graded ferroelectric might induce some change in the free-carrier concentration and the magnitude of the band gap along the growth direction.[17] Those could lead to asymmetric conductivity within the film.

All in all, we have investigated the effect of asymmetric conductivity in both horizontal and vertical shifts in hysteresis loops of ferroelectric films. It has been found that a bulk sample with zero conductivity does not give any vertical shift.[28] The case of negligible conductivity can also be examined for a bilayer structure with different polarization loops for the constituents. Using the analytical expressions obtained from Eqs. (8)–(10) for the ferroelectric-ferroelectric structure and considering the case $\sigma_f^\pm = \sigma_d^\pm = 0$, we found that in a looping cycle, only six paths (out of a total of 36) would give a zero vertical shift, i.e.,

$$\int_{t_{Ea}^{+}}^{t_{Ea}^{+}+T} D_f(t)dt = 0. \tag{12}$$

These paths are listed in the Appendix. In other words, for looping without polarization shift, if the path for decreasing field is "$E(t_{Ea}^{+}) \rightarrow e_1 \rightarrow e_2 \rightarrow e_3 \rightarrow e_4 \rightarrow E(t_{Ea}^{-})$" (symbol $e$ represents the critical electric fields in Fig. 2), then the path for the subsequent increasing field must be "$E(t_{Ea}^{-}) \rightarrow -e_1 \rightarrow -e_2 \rightarrow -e_3 \rightarrow -e_4 \rightarrow E(t_{Ea}^{+}+T)$." For example, Eq. (12) is satisfied for the path "$E(t_{Ea}^{+}) \rightarrow -E_{c,1}^{-} \rightarrow -E_{c,2}^{-} \rightarrow -E_{c,1}^{+} \rightarrow -E_{c,2}^{+} \rightarrow E(t_{Ea}^{-}) \rightarrow E_{c,1}^{-} \rightarrow E_{c,2}^{-} \rightarrow E_{c,1}^{+} \rightarrow E_{c,2}^{+} \rightarrow E(t_{Ea}^{+}+T)$," but not for "$E(t_{Ea}^{+}) \rightarrow -E_{c,1}^{-} \rightarrow -E_{c,2}^{-} \rightarrow -E_{c,1}^{+} \rightarrow -E_{c,2}^{+} \rightarrow E(t_{Ea}^{-}) \rightarrow E_{c,2}^{-} \rightarrow E_{c,1}^{-} \rightarrow E_{c,2}^{+} \rightarrow E_{c,1}^{+} \rightarrow E(t_{Ea}^{+}+T)$." This suggests that, generally in a bilayer structure with negligible conductivity, if the "order" of switching in the constituents (which is mainly governed by the different loop size of the constituents) for decreasing (from $t_{Ea}^{+}$ to $t_{Ea}^{-}$) and increasing field (from $t_{Ea}^{-}$ to $t_{Ea}^{+}+T$) is identical, no polarization offset will result. Indeed, we have also found that this hypothesis remains valid for other loop shapes, as we have numerically performed the above analysis with a more realistic hysteresis model of a different loop shape.[30] On the other hand, when the $P$-$E$ hysteresis loop of each constituent has a "symmetric" shape, i.e., $P(E) = -P(-E)$, for the increasing and decreasing field branches, Eq. (12) seems to be satisfied for any combination of the constituents. Hence, it seems quite impossible to obtain polarization offset in a bilayer with no conductivity.

Our ferroelectric–ferroelectric layered model can readily be used to study the effect of a stepped polarization gradient on the ferroelectric behavior in graded ferroelectrics. For materials with a smoother polarization gradient, a multilayered structure[30] with a sufficient number of layers should be employed. On the other hand, our analytical formulation is also suitable for the study of the behavior of other ferroelectric layered structures. For example, by using proper boundary conditions, our current formalism may be extended to study the hysteresis behavior of ferroelectric superlattices.[31]

## IV. CONCLUSIONS

We have modeled a thin ferroelectric film with a passive layer using a bilayer ferroelectric–dielectric or ferroelectric-ferroelectric structure. The horizontal shift of hysteresis loops observed experimentally can be reproduced by setting asymmetric conductivity in the passive layer. This experimental phenomenon cannot be reproduced by this model if only a nonferroelectric second phase with zero conductivity or an average asymmetric conductivity across the bilayer structure (which is conventionally measured experimentally) is assumed. Unlike some existing models in the literature, our modeled results can cover a very broad range of shift magnitudes, sometimes up to very large magnitudes. We find that a large amplitude of the applied field, a thicker passive layer, and a larger asymmetry of conductivity in the passive layer enhance the effect of horizontal offset. The present model is not limited to discuss the effect of horizontal shifts. By setting asymmetric conductivity in the bulk layer, anomalous vertical shifts similar to that in graded ferroelectrics are obtained. In summary, asymmetric conductivity at film–electrode interface (dead layer) produces horizontal shifts (i.e., imprint behavior), while the same within the film vertical shifts are produced (i.e., graded ferroelectric behavior).

## ACKNOWLEDGMENT

This work was partially supported by the Center for Smart Materials of The Hong Kong Polytechnic University.

## APPENDIX

The six paths in the looping regimes of Fig. 2 (out of a total of 36) that satisfy Eq. (12) are

(1)
$$E(t_{Ea}^{+}) \rightarrow -E_{c,1}^{-} \rightarrow -E_{c,1}^{+} \rightarrow -E_{c,2}^{-} \rightarrow -E_{c,2}^{+} \rightarrow E(t_{Ea}^{-}) \rightarrow E_{c,1}^{-} \rightarrow E_{c,1}^{+} \rightarrow E_{c,2}^{-} \rightarrow E_{c,2}^{+} \rightarrow E(t_{Ea}^{+}+T),$$

(2)
$$E(t_{Ea}^{+}) \rightarrow -E_{c,1}^{-} \rightarrow -E_{c,2}^{-} \rightarrow -E_{c,1}^{+} \rightarrow -E_{c,2}^{+} \rightarrow E(t_{Ea}^{-}) \rightarrow E_{c,1}^{-} \rightarrow E_{c,2}^{-} \rightarrow E_{c,1}^{+} \rightarrow E_{c,2}^{+} \rightarrow E(t_{Ea}^{+}+T),$$

(3)
$$E(t_{Ea}^{+}) \rightarrow -E_{c,1}^{-} \rightarrow -E_{c,2}^{-} \rightarrow -E_{c,2}^{+} \rightarrow -E_{c,1}^{+} \rightarrow E(t_{Ea}^{-}) \rightarrow E_{c,1}^{-} \rightarrow E_{c,2}^{-} \rightarrow E_{c,2}^{+} \rightarrow E_{c,1}^{+} \rightarrow E(t_{Ea}^{+}+T),$$

(4)
$$E(t_{Ea}^{+}) \rightarrow -E_{c,2}^{-} \rightarrow -E_{c,1}^{-} \rightarrow -E_{c,1}^{+} \rightarrow -E_{c,2}^{+} \rightarrow E(t_{Ea}^{-}) \rightarrow E_{c,2}^{-} \rightarrow E_{c,1}^{-} \rightarrow E_{c,1}^{+} \rightarrow E_{c,2}^{+} \rightarrow E(t_{Ea}^{+}+T),$$

(5)
$$E(t_{Ea}^{+}) \rightarrow -E_{c,2}^{-} \rightarrow -E_{c,1}^{-} \rightarrow -E_{c,2}^{+} \rightarrow -E_{c,1}^{+} \rightarrow E(t_{Ea}^{-}) \rightarrow E_{c,2}^{-} \rightarrow E_{c,1}^{-} \rightarrow E_{c,2}^{+} \rightarrow E_{c,1}^{+} \rightarrow E(t_{Ea}^{+}+T),$$

(6)
$$E(t_{Ea}^{+}) \rightarrow -E_{c,2}^{-} \rightarrow -E_{c,2}^{+} \rightarrow -E_{c,1}^{-} \rightarrow -E_{c,1}^{+} \rightarrow E(t_{Ea}^{-}) \rightarrow E_{c,2}^{-} \rightarrow E_{c,2}^{+} \rightarrow E_{c,1}^{-} \rightarrow E_{c,1}^{+} \rightarrow E(t_{Ea}^{+}+T).$$

[1] W. L. Warren, G. E. Pike, B. A. Tuttle, and D. Dimos, Appl. Phys. Lett. **70**, 2010 (1997).
[2] E. G. Lee, D. J. Wouters, G. Willems, and H. E. Maes, Appl. Phys. Lett. **69**, 1223 (1996).
[3] B. H. Park, T. W. Noh, J. Lee, C. Y. Kim, and W. Jo, Appl. Phys. Lett. **70**, 1101 (1997).
[4] S. Okamura, S. Miyata, Y. Mizutami, T. Nishida, and T. Shiosaki, Jpn. J. Appl. Phys., Part 1 **38**, 5364 (1999).
[5] D. Nagasawa and H. Nozawa, Jpn. J. Appl. Phys., Part 1 **38**, 5406 (1999).
[6] W. Liu, J. Ko, and W. Zhu, Mater. Lett. **49**, 122 (2001).
[7] Y. Xu, C. J. Chen, R. Xu, and J. D. Mackenzie, J. Appl. Phys. **67**, 2985 (1990).
[8] S. K. Dey, J. J. Lee, and P. Alluri, Jpn. J. Appl. Phys., Part 1 **34**, 3142 (1995).
[9] J. J. Lee and S. B. Desu, Ferroelectr., Lett. Sect. **20**, 27 (1995).
[10] U. Robels, J. H. Calderwood, and G. Arlt, J. Appl. Phys. **77**, 4002 (1995).
[11] K. Abe, N. Yanase, T. Yasumoto, and T. Kawakubo, Jpn. J. Appl. Phys., Part 1 **41**, 6065 (2002).
[12] T. Lü and W. Cao, Microelectron. Eng. **66**, 818 (2003).
[13] L. Baudry, J. Appl. Phys. **86**, 1096 (1999).
[14] K. W. Lee, Y. I. Kim, and W. J. Lee, Ferroelectrics **271**, 1769 (2002).
[15] V. C. Lo and Z. J. Chen, IEEE Trans. Ultrason. Ferroelectr. Freq. Control **49**, 980 (2002).
[16] G. Poullain, R. Bouregba, B. Vilquin, G. Le Rhun, and H. Murray, Appl. Phys. Lett. **81**, 5015 (2002).
[17] R. Bouregba, G. Poullain, B. Vilquin, and G. Le Rhun, J. Appl. Phys. **93**, 5583 (2003).
[18] H. K. Chan, C. H. Lam, and F. G. Shin, J. Appl. Phys. **95**, 2665 (2004).
[19] Y. Watanabe, D. Sawamura, and M. Okano, Solid State Ionics **108**, 109 (1998).
[20] C. Yoshida, A. Yoshida, and H. Tamura, Appl. Phys. Lett. **75**, 1449 (1999).
[21] R. Bouregba and G. Poullain, J. Appl. Phys. **93**, 522 (2003).

[22]C. Zhou and D. M. Newns, J. Appl. Phys. **82**, 3081 (1997).
[23]S. L. Miller, J. R. Schwank, R. D. Nasby, and M. S. Rodgers, J. Appl. Phys. **70**, 2849 (1991).
[24]L. Zheng, C. Lin, W.-P. Xu, and M. Okuyama, J. Appl. Phys. **79**, 8634 (1996).
[25]R. M. Corless, G. H. Gonnet, D. E. G. Hare, D. J. Jeffrey, and D. E. Knuth, Adv. Comput. Math. **5**, 329 (1996).
[26]R. Bouregba, G. Poullain, B. Vilquin, and H. Murray, Ferroelectrics **256**, 47 (2001).
[27]B. Chen, H. Yang, L. Zhao, J. Miao, B. Xu, X. G. Qiu, B. R. Zhao, X. Y. Qi, and X. F. Duan, Appl. Phys. Lett. **84**, 583 (2004).
[28]C. K. Wong, C. H. Tsang, and F. G. Shin, J. Appl. Phys. **96**, 575 (2004).
[29]M. Brazier, M. McElfresh, and S. Mansour, Appl. Phys. Lett. **72**, 1121 (1998).
[30]Y. T. Or, C. K. Wong, B. Ploss, and F. G. Shin, J. Appl. Phys. **93**, 4112 (2003).
[31]T. Shimuta, O. Nakagawara, T. Makino, S. Arai, H. Tabata, and T. Kawai, J. Appl. Phys. **91**, 2290 (2002).